Structure and Stability of the Endohedrally Doped $(X@CdiSi)^{q=0,1}_{i=4,9,12,15,16}$, X=Na, K, Cl, Br, Nanoclusters

Elisa Jimenez-Izal,* Jon M. Matxain, Mario Piris, and Jesus M. Ugalde

Kimika Fakultatea, Euskal Herriko Unibertsitatea and Donostia International Physics Center (DIPC), P.K. 1072, 20018 Donostia, Euskadi Spain

Endohedral $(X@CdiSi)_i^{q=0,1}$ structures have been characterized by means of the density functional theory, with X being alkali metals such as Na and K or halogens such as Cl and Br and with i = 4, 9, 12, 15, 16. These nanoclusters have been chosen because of their high sphericity, which is known to be one of the parameters determining the stability of the endohedral nanoclusters, along with the charge and size of the guest atom. In these structures, the atoms are trapped inside previously characterized spheroid hollow structures with positively charged Cd atoms and negatively charged S atoms. Moreover, although the radii of all atoms are similar, Cd atoms are located more inside the structure. For alkali metals, neutral and cationic endohedral compounds have been characterized and, for halogens, neutral and anionic nanoclusters have been characterized.It is observed that some of these guest atoms are trapped in the center of mass of the cluster, while others are found to be displaced from that center leading to structures where the guest atom presents a complex dynamical behavior. This fact was confirmed by quantum molecular dynamics calculations, which further confirmed the thermal stability of these endohedral compounds.

INTRODUCTION

Nanostructured materials have fundamental and technological importance for their novel structural, physical, and chemical properties, which usually differ markedly with respect to those of their corresponding bulk material. Since these properties vary with the size of the nanoparticle, materials with modified properties can in principle be obtained. Size control, therefore, appears crucial at this point to monitor and stabilize the targeted physical property, and much effort has been dedicated toward this goal in the past decade. (1)

Concomitantly, on-purpose modification of the physical and chemical properties of nanoparticles can be achieved by doping. In this vein, spherical hollow clusters provide the chance for endohedral doping, namely, the dopant is placed in the interior of the cavity of the hollow nanoparticle.

The first endohedrally doped nanoparticles described as such in the literature were several endohedral fullerenes. (2-7) Later, it was found that elements other than carbon may also be used to build hollow structures with sufficient space to trap guest atoms. As a matter of fact, endohedrally doped nanoclusters of gold, (8) tin, (9-11) lead, (12, 13, 11) and germanium (14-16) have been reported recently.

Hollow binary nanoclusters of II−VI semiconductor elements have also been widely studied in the literature both theoretically and experimentally. (17-25) However, studies of the properties of endohedral compounds made of these hollow nanoclusters are scarce. (26, 27) Of particular relevance to the present research is the previous characterization of the $(X@Zn_iSi_i)_{i=4-16}^{0,\pm1}$ compounds (28) with X being alkali metals or halogens. In this work, it was observed that alkali metals transferred an electron to the cage, while halogen atoms took an electron from the cage leading to charged ions inside the cage. Moreover, encapsulation of halogen atoms resulted in endohedral nanoclusters with enhanced electron affinity relative to the guest halogen atom (4.5 eV compared to 3.5 eV). These nanoclusters ought, therefore, to be considered as superhalogens in the same vein as the $Al@Al_{12}$ cluster for which recent research has confirmed its predicted (29) high electron affinity (EA) of 3.20 eV as well as its ability to ionize spontaneously into $(Al@Al_{12})^-K^+$ in the gas phase. (30)

The Cl and Br endohedral nanoclusters studied in ref 28 have electron affinities substantially larger than $Al@Al_{12}$. Hence, they are expected to have even a stronger superhalogen character. Furthermore, the electron affinities of the halogen endohedral nanoclusters and the ionization energies of the alkali endohedral nanoclusters of Zn_iS_i are rather similar rendering them good candidates to form cluster-assembled materials under mild conditions since large ionization energy/electron affinity (IE/EA) differences would yield substantial heat release during assembling that might destroy the assembled material as it is formed. Such solids, based on $X@Zn_{12}S_{12}$ structures, have been recently theoretically characterized. (31) They have face-centered cubic (fcc) crystal lattice structure, and interestingly, the band gap is decreased from 3.66 eV found in wurtzite to 2.2 eV in the bare solid and even further, to 1.8 eV, in the doped solids. These solids may be seen as semiconducting materials with smaller band gaps than the solids found in nature, namely, wurtzite and zinkblende. Ab initio quantum dynamics calculations further confirmed the thermal stability of the calculated structures. Moreover, the predicted metastability of the fcc structures was supported by the predicted energy barriers toward collapsing into wurtzite, which were found to be larger than 6 eV.

The potential technological applications of these newly designed materials in a large variety of fields, like solar cells, heterogeneous catalysis, molecular transport, optical sensors, and so on, make the searching of new building blocks for such materials worthwhile. Within this context, the theoretical investigations reported herein could help, or guide, experimentalists toward such a goal.

Thus, Cd_iS_i, i = 1−16, clusters have been synthesized and characterized by Sanville et al. (24) Consequently, one could think of using these clusters as building blocks to synthesize new stable molecular solids. However, we propose that using endohedrally doped selected Cd_iS_i hollow clusters should represent a wiser choice because (1) the stability of the cluster structures

themselves are not compromised by the endohedral doping and (2) a larger variety of properties can be tailored by such doping.

Herein, we will describe the physicochemical properties of $(X@Cd_iS_i)^q$ i=4,9,12,15,16 and q=0,±1 clusters, with X = Na, K, Cl, Br, on the basis of our density functional theory (DFT) and quantum molecular simulation calculations. These clusters were chosen because of their hollow spherical shape, which is one main parameter determining their stability.

Our results, along with the earlier mentioned work by Sanville et al. and the related experimental work on cadmium chalcogenide stoichiometric hollow clusters by Kasuya et al. (25, 32) and by Riehle et al., (33) suggest that these hypothetical clusterlike compounds could be within experimental reach in the near future.

METHODS

All geometries have been fully optimized using the gradient-corrected hybrid B3LYP (34-36) functional within the Kohn−Sham implementation (37) of density functional theory. (38) Harmonic vibrational frequencies are determined by analytical differentiation of gradients to determine whether the structures found are true minima or not and to extract zero-point energies and Gibbs free energy contributions.

The relativistic compact effective core potentials and shared-exponent basis set (39) of Stevens et al. were used for Cd and S, as in the study of the isolated clusters, (22) and the all-electron 6-311+G(d) basis set was used for the trapped atom. The 4d electrons of Cd were included in the valence. To perform the geometry optimizations and harmonic frequency calculations, an extra d function was added on Cd and S because of its importance for the proper description of the high coordination of the atoms in the three-dimensional cluster structures. Pure angular momentum functions were used throughout this study.

To further explore the thermal stability of these compounds, we also undertook ab initio thermal molecular dynamics (MD) simulations at 298 K on the calculated local minima structures controlled by means of the Nose thermostat as implemented in the SIESTA code (40) within DFT approach. Exchange and correlation effects were described using the generalized gradient approximation (GGA) within the revised Perdew−Burke−Ernzerhof (rPBE) functional. (41-43) Core electrons were replaced by Troullier−Martins norm-conserving pseudopotentials (44) in the Kleinman−Bylander factorized form. (45) In the context of SIESTA, the use of pseudopotentials imposes basis orbitals adapted to them. Furthermore, SIESTA employs a localized basis set to represent the Kohn−Sham orbitals for valence electrons. Accordingly, the basis set of atomic orbitals is constructed from numerical solutions of the atomic pseudopotential and are constrained to be zero beyond a cutoff radius. We used a basis set of double- ζ plus polarization quality (DZP). A single parameter, orbital energy shift (ΔE_{PAO}), defines the confinement radii of different orbitals. With this basis set, SIESTA calculates the self-consistent potential on a grid in real space. The fineness of this grid is determined in terms of an energy cutoff (E_{cutoff}) in analogy to the energy cutoff when the basis set involves plane waves. We have first checked the influence of the ΔE_{PAO} and E_{cutoff} parameters for different endohedral compounds. These values are set to ΔE_{PAO} = 150 meV and E_{cutoff} = 200 Ry in routine calculations, but in addition to this, we

have carried out the quantum dynamics simulations for ΔE_{PAO} = 50 meV and E_{cutoff} = 200 Ry, and ΔE_{PAO} = 50 meV and E_{cutoff} = 300 Ry, to check the influence for both parameters on the obtained results. Notice that the smaller the ΔE_{PAO} value and the larger the E_{cutoff} value the more accurate the calculation.

To analyze the effect of the orbital energy shift and the mesh cutoff, we have focused on X@$Cd_{12}S_{12}$ endohedral nanoclusters with X = Na, K, Cl, and Br. The effect of changing ΔE_{PAO} and E_{cutoff} appears to be dramatical for the smallest atom, Na, as can be seen in Figure 1. There, the distances of the Na atom with respect to the center of mass of the nanocluster and the total energy along the simulations are depicted for three different cases mentioned above. One may observe that for ΔE_{PAO} = 150 meV and E_{cutoff} = 200 Ry, the endohedral Na@$Cd_{12}S_{12}$ structure is not altered, the Na atom moves near the center of the nanocluster, and the total energy oscillates around the same value. However, more fine calculations, with ΔE_{PAO} = 50 meV and E_{cutoff} = 200 Ry, show that Na atom moves from the center toward the surface of the nanocluster, which leads to a more stable structure, as can be seen in the total energy picture. This is due to the small size of sodium compared to the cavity available in the nanocluster, which allows it to move close to the surface interacting covalently with it. Further increase in E_{cutoff} has no influence in the final result, and thus calculations using ΔE_{PAO} = 50 meV and E_{cutoff} = 300 Ry do not produce any change in the dynamics. For larger trapped atoms, namely, K, Cl, and Br, we have observed that changing ΔE_{PAO} and E_{cutoff} does not alter the final result (see Supporting Information).We therefore conclude that endohedral Na@Cd_iS_i compounds need a higher degree of fineness in the calculations. Therefore, ab initio quantum dynamics calculations have been carried out with ΔE_{PAO} = 50 meV and E_{cutoff} = 200 Ry for X = Na and with ΔE_{PAO} = 150 meV and E_{cutoff} = 200 Ry for the rest to save computational resources. All these simulations were carried out for 6 ps with a chosen time step of 1 fs.

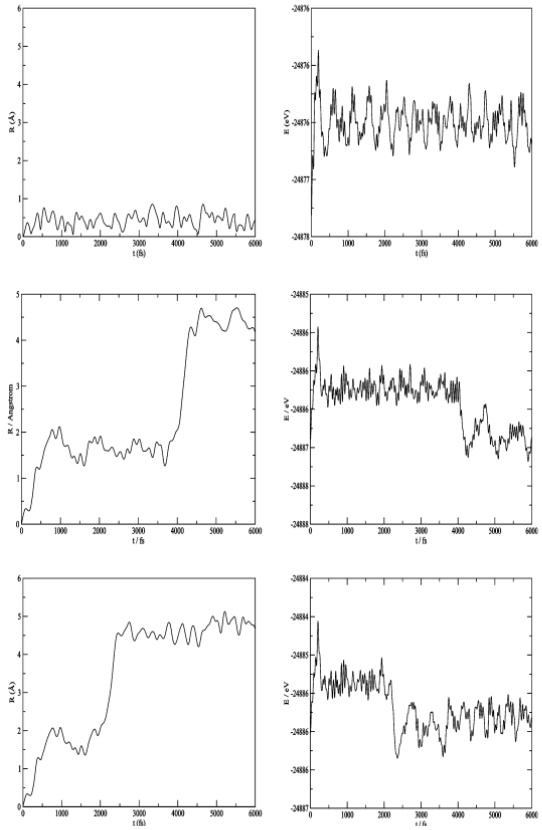

Figure 1. The distance of the Na atom from the center of mass of the $Cd_{12}S_{12}$ nanocluster, in Å, and the total energy of the endohedral $Na@Cd_{12}S_{12}$ nanocluster as a function of the simulation time, in fs, for three different choices of the ΔE_{PAO} and E_{cutoff} parameters. Top panels: ΔE_{PAO} = 150 meV and E_{cutoff} = 200 Ry. Middle pannels: ΔE_{PAO} = 50 meV and E_{cutoff} = 200 Ry. Bottom panels: ΔE_{PAO} = 50 meV and E_{cutoff} = 300 Ry.

RESULTS

First, the effect of the charge on the geometry of the bare nanoclusters will be analyzed. We anticipate that the most salient geometrical feature of the charged nanoclusters is that the size of the cavity, as compared to their neutral counterparts, changes noticeably. The ionization energies and the electron affinities of the bare nanoclusters will also be discussed. Then, we will focus on the endohedral compounds. Both neutral and cationic nanoclusters have been found to be able to encapsulate alkali metals. Halogen atoms, on the other hand, can be encapsulated by the neutral and anionic nanoclusters.

First, the structures of charged and neutral endohedral nanoclusters will be characterized and their properties analyzed. Then, ab initio molecular dynamics simulations will be carried out to assess the thermal stability of these compounds.

Bare Nanoclusters and Atoms

The structures of the cationic and anionic bare nanoclusters were characterized first. Starting from the neutral nanoclusters, an electron was either removed (for the cations) or added (for the anions) followed by geometry optimizations and frequency calculations to obtain and characterize the optimized structures of the nanocluster ions. For the structures, the adiabatic ionization energies (IE) and electron affinities (EA) were calculated. The structures of the cationic and anionic nanoclusters followed the well-known square-hexagon rule as do their neutral counterparts.

In Table 1, the average radii of the sphere defined by the Cd atoms, *r*Cd, their standard deviation, and the cavity of the cluster, r_{cavity}, are given along with ionization energies (IE) and electron affinities (EA) for the neutral clusters. The radius of the cavity inside the spheroidal nanoclusters is defined by the Cd atoms (see ref 28) and is given by $r_{cavity} = r_{Cd} - r_{Cd+2}^{ionic}$, with $r_{Cd}^{+2ionic} = 0.97$ Å. r_{cavity} is given for all the neutral, cationic, and anionic nanoclusters. Notice that, compared with the neutral structures, cationic r_{cavity} values are slightly affected while anionic ones are significantly increased. Recall that Cd atoms, which are located more inside the structure, have positive partial charges of ~1*e*, while S atoms have negative partial charge of ~−1*e*.

Table 1. Average Radii of the Sphere Defined by the Cd Atoms, r_{Cd}, the Standard Deviation (σ), the Cavity inside the Clusters, r_{cavity}, in Å, and the Ionization Potentials (IE) and Electron Affinities (EA) in eV.

				r_{cavity}		
i	IE	EA	r_{Cd} (σ)	$q = 0$	$q = 1$	$q = -1$
4	7.85	2.35	1.95 (0.00)	0.98	0.98	1.04
9	7.80	2.45	3.12 (0.18)	2.15	2.17	2.20
12	7.90	2.50	3.62 (0.00)	2.65	2.68	2.71
15	7.69	2.67	4.11 (0.37)	3.14	3.14	3.17
16	7.68	2.71	4.24 (0.09)	3.27	3.29	3.30

Comparing r_{cavity} for the neutral and ionic nanoclusters, we can conclude that r_{cavity} in general stays constant in cationic clusters but increases from neutral to anionic structures. The maximum increase is 0.06 Å.

However, the sphericity of the nanoclusters is not the same. A way of measuring the sphericity of these clusters is the standard deviation (σ) of the distances between the Cd atoms and the center of the nanoclusters. The smaller the σ, the more spherical the nanocluster is. The structures of the cationic and anionic nanoclusters retain the sphericity of their neutral counterparts. It may be seen that Cd_iS_i nanoclusters with i = 4, 12, 16 have σ ≃ 0 and are almost fully spherical. The i = 9 nanocluster has only a small sphericity deviation (σ = 0.15). Hence, all these nanoclusters are highly spherical. However, the case of $Cd_{15}S_{15}$ is particular which, with a σ = 0.37, is far from sphericity. Nevertheless, this structure is highly symmetric. It resembles a

rugby ball, which is symmetric but the distances to the center of the ball are not the same. The significance of this particular structure will be clarified later.

The ionization energies of these clusters oscillate around 7.8 eV, and the electron affinities oscillate around 2.5 eV. These values are indicative of the high stability of the neutral bare nanoclusters.

Endohedral Nanoclusters

We have considered all possible $(X@Cd_iS_i)^q$ endohedral compounds with i = 4, 9, 12, 15, 16; q = 0, 1, −1; and X = Na, K, Cl, Br. As seen in the Methods section, ab initio quantum molecular dynamics calculations show that sodium atoms move toward the surface in $Cd_{12}S_{12}$. This is indicative of the low thermal stability of these compounds. For other sodium-doped nanoclusters, similar behavior has been observed, and consequently, we focus the discussion on the thermally stable $K@Cd_iS_i$, $Cl@Cd_iS_i$, and $Br@Cd_iS_i$ nanoclusters. Information about the thermally unstable $Na@Cd_iS_i$ local minima is available in the Supporting Information.

The thermodynamic stability of the minima will be assessed by the free energy of encapsulation (ΔGinc) defined by the following reaction:

$$Cd_iS_i + X^q \rightarrow (X@Cd_iS_i)^q \quad q = 0, \pm 1$$

A negative value of ΔG_{inc} indicates that the endohedral nanocluster is thermodynamically more stable than the separated fragments. In Figure 2, the characterized $X@Cd_iS_i$ endohedral nanoclusters are shown. For the sake of clarity, K and halogen (Cl, Br) endohedral nanoclusters will be discussed separately.

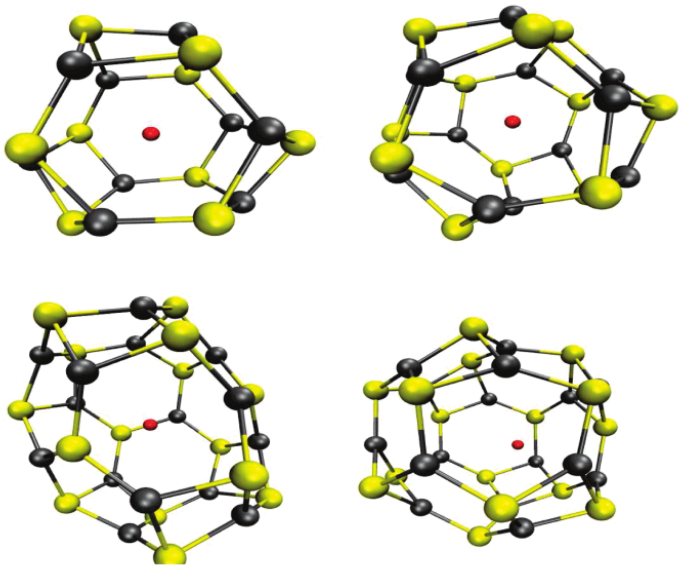

Figure 2. Structures of $X@Cd_9S_9$, $X@Cd_{12}S_{12}$, $X@Cd_{15}S_{15}$, and $X@Cd_{16}S_{16}$, X = K, Cl, Br. S atoms are drawn in yellow, while Cd atoms are drawn in gray.

K@Cd$_i$S$_i$ Endohedral Nanoclusters

In Table 2, the geometric, electronic, and energetic properties of the characterized local minima of K@Cd$_i$S$_i$ endohedral nanoclusters are given. In addition, the R_{range}^{dyn} and R_{av}^{dyn} geometrical parameters, representative of the dynamic movement of the trapped potassium atom inside the nanocluster, are given. *R*rangedyn denotes the range of the distance between the trapped atom and the center of the nanocluster, while R_{av}^{dyn} is the average distance of the trapped atom with respect to the center of the nanocluster along the simulation time.

Table 2. Cavity within the Cluster (r_{cavity}); the Distance of the Guest Atom with Respect to the Center of the Cluster in Å; the Free Energy of Complexation, Δ*G*inc, in kcal/mol; the Charge of the Endohedral Atom, q_x; and the Ionization Energies in eV.

	r_{cavity}	R^{LM}	R_{range}^{dyn}	R_{av}^{dyn}	ΔG_{inc}	q_x	IE
K@Cd$_9$S$_9$	2.41	0.00	0.00−0.62	0.23 (0.11)	−4.78	0.21	5.74
K@Cd$_{12}$S$_{12}$	2.83	0.00	0.00−0.67	0.30 (0.13)	−12.40	0.29	5.50
K@Cd$_{15}$S$_{15}$	3.29	0.00	0.00−1.39	0.66 (0.32)	−16.45	0.25	5.24
K@Cd$_{16}$S$_{16}$	3.40	1.77	0.05−1.17	0.70 (0.25)	−14.26	0.40	5.50
(K@Cd$_9$S$_9$)$^+$	2.35	0.00	0.00−0.44	0.19 (0.07)	23.80	0.38	
(K@Cd$_{12}$S$_{12}$)$^+$	2.79	0.00	0.00−0.55	0.27 (0.12)	10.79	0.51	
(K@Cd$_{15}$S$_{15}$)$^+$	3.26	0.00	0.00−1.15	0.52 (0.25)	0.60	0.52	
(K@Cd$_{16}$S$_{16}$)$^+$	3.37	1.50	0.09−1.52	0.62 (0.28)	8.85	0.51	

[a]*R*LM for the stationary local minima; R_{range}^{dyn} and R_{av}^{dyn}: the range and average position in the dynamic simulation.

Minima structures are found for both neutral and cationic endohedral structures for *i* = 9, 12, 15, 16. In all structures, K is positively charged but a bit more for cationic compounds than in neutral ones. In the former case, the Coulombic repulsion between the trapped K atom and the Cd atoms is larger than in the latter, which dramatically affects the calculated encapsulation free energies, ΔG_{inc}. They are negative for neutral compounds and positive for the cationic endohedral nanoclusters. Hence, cationic compounds are predicted to be thermodynamically unstable with respect to their corresponding separated compounds. Nonetheless, the height of the barrier for the evaporation of potassium atoms might render these complexes with long enough lifetimes to be amenable to experimental detection. In general, in both neutral and cationic compounds, free energy indicates that the compounds are thermodynamically more stable as the size of the nanoclusters increases. This is due to a combination of two factors, namely, the better size fit of the K atom inside the cavity and the smaller Coulombic repulsion between K and Cd atoms. S atoms are located at a longer distance from the center, and therefore, locally the K−Cd interaction prevails. These arguments also account for the fact that when the size of the cluster increases, the cavity radii is less affected and consequently remains almost constant. The largest increase of cavity compared to the bare case occurs for K@Cd$_9$S$_9$, while the smallest increase occurs for K@Cd$_{16}$S$_{16}$. In these nanoclusters, K atom lies at the center of the structure except in neutral and cationic K@Cd$_{16}$S$_{16}$ structures which are too big to

keep the guest atom in the center of the cluster. In addition to this, endohedral K doping of the Cd_iS_i nanoclusters lowers the ionization energy from ~7.8 eV to a value between 5.24 and 5.74 eV, which is similar to that of potassium atom and $K@Zn_iS_i$ nanoclusters.

The ab initio quantum dynamics simulations of these compounds reveal that the trapped atom moves around the center of the nanocluster as shown by the values of R_{range}^{dyn} and R_{av}^{dyn} given in Table 2. Since the dynamics of all compounds are similar, for discussion, we focus on $K@Cd_{12}S_{12}$, and the information about the remaining compounds are given in the Supporting Information. In Figure 3, it is observed that the total energy oscillates around the same value during the simulation time and that the K atom moves around the center of the nanocluster all along the simulation. Therefore, these nanoclusters are predicted to be thermally stable enough to survive long enough at room temperature to allow for their experimental detection.

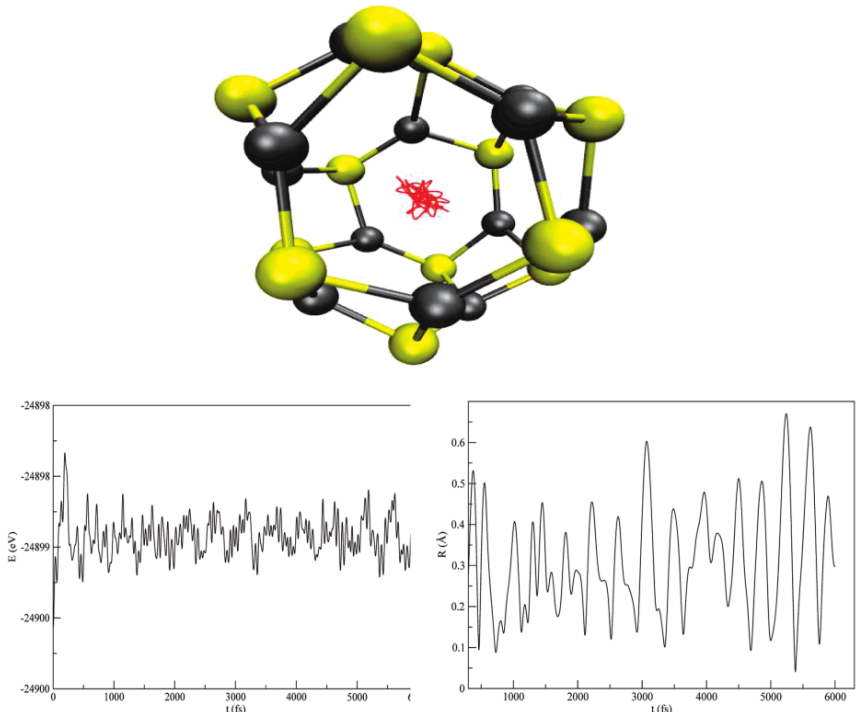

Figure 3. Dynamics simulation of $K@Cd_{12}S_{12}$. Top: Dynamical trajectories of the K atom inside the nanocluster. This plot was prepared as follows. For each saved structure along the dynamics, the center of mass of the spheroid was set on the origin, and the coordinates of all atoms in the system referred to this center of mass. Then, the average position for each of the atoms of the spheroid along the dynamics was calculated, and the corresponding average spheroid structure is the one shown in the figure. Finally, the red line corresponds to the positions of the inner atom (K) with respect to the center of mass of the spheroid for each saved structure. Bottom: The variation of the energy, in eV (left), and the variation of the distance, *R*, in Å (right), of the trapped K atom from the center of mass of the nanocluster as a function of time. S atoms are drawn in yellow, while Cd atoms are drawn in gray.

Cl@Cd*i*S*i* and Br@Cd*i*S*i* Endohedral Nanoclusters

Table 3 shows the geometric, electronic, and energetic properties of the characterized local minima of the endohedral neutral and anionic Cl@Cd_iS_i, and Br@Cd_iS_i endohedral nanoclusters are given. In addition, the R_{range}^{dyn} and R_{av}^{dyn} parameters, as representatives of the dynamics of the trapped atoms inside the nanocluster, are also shown.

Table 3. Cavity within the Cluster (r_{cavity}); the Distance of the Guest Atom with Respect to the Center of the Cluster in Å; the Free Energy of Complexation, ΔG_{inc}, in kcal/mol; the Charge of the Endohedral Atom, q_x; and the Ionization Energies, in eV.

	r_{cavity}	R^{LM}	R_{range}^{dyn}	R_{av}^{dyn}	ΔG_{inc}	q_x	EA
$Cl@Cd_9S_9$	2.12	0.10	0.02−0.31	0.12 (0.05)	−31.53	−0.69	4.66
$Cl@Cd_{12}S_{12}$	2.57	0.33	0.03−0.66	0.30 (0.12)	−44.08	−0.60	5.11
$Cl@Cd_{15}S_{15}$	3.05	0.81	0.15−1.50	0.69 (0.30)	−47.33	−0.60	5.15
$Cl@Cd_{16}S_{16}$	3.18	1.11	0.59−1.59	1.08 (0.21)	−48.87	−0.61	4.96
$(Cl@Cd_9S_9)^-$	2.11	0.00	0.00−0.33	0.12 (0.05)	−53.20	−0.79	
$(Cl@Cd_{12}S_{12})^-$	2.56	0.00	0.00−39	0.20 (0.08)	−76.13	−0.75	
$(Cl@Cd_{15}S_{15})^-$	3.03	0.14	0.03−1.40	0.73 (0.28)	−80.14	−0.72	
$(Cl@Cd_{16}S_{16})^-$	3.17	1.02	0.52−1.48	1.05 (0.19)	−77.29	−0.70	
$Br@Cd_9S_9$	2.16	0.09	0.02−0.29	0.14 (0.06)	−7.42	−0.67	4.68
$Br@Cd_{12}S_{12}$	2.59	0.21	0.02−0.53	0.26 (0.10)	−31.64	−0.61	5.13
$Br@Cd_{15}S_{15}$	3.04	0.09	0.03−0.97	0.56 (0.21)	−33.76	−0.51	5.31
$Br@Cd_{16}S_{16}$	3.18	0.83	0.21−1.31	0.76 (0.21)	−39.17	−0.62	5.10
$(Br@Cd_9S_9)^-$	2.14	0.00	0.00−0.31	0.14 (0.06)	−32.45	−0.78	
$(Br@Cd_{12}S_{12})^-$	2.57	0.00	0.00−0.29	0.18 (0.06)	−67.13	−0.77	
$(Br@Cd_{15}S_{15})^-$	3.04	0.00	0.00−0.87	0.54 (0.20)	−73.36	−0.73	
$(Br@Cd_{16}S_{16})^-$	3.17	0.51	0.07−1.38	0.69 (0.22)	−73.80	−0.71	

[a] *R*LM for the stationary local minima; R_{range}^{dyn} and R_{av}^{dyn}: the range and average position in the dynamic simulation.

Cl and Br can be trapped by Cd_iS_i (i = 9, 12, 15, 16) nanoclusters to yield neutral and anionic species. In all structures, Cl and Br are negatively charged. Notice that q_x is predicted to be more negative for the anionic endohedral compounds. In the latter, the Coulombic attraction between the trapped halogen atom and the Cd atoms increases. This affects noticeably the calculated encapsulation free energies, ΔG_{inc}, which are found to be negative in all cases because of the attractive interactions but are more negative for the anionic species because of the larger Coulombic interaction. These compounds are predicted to be thermodynamically stable with respect to their corresponding separated compounds. Moreover, in both neutral and anionic compounds, free energy indicates that the compounds are thermodynamically more stable as the size of the nanoclusters increases. This is due to a combination of two factors, namely, the better size fit of the halogen atoms inside the cavity and the larger Coulombic attraction between these and Cd atoms. These same arguments explain also why the cavity radii are contracted upon halogen encapsulation and why this contraction is larger for large

clusters. For these nanoclusters, the halogen atoms lie at the center or near the center of the nanocluster except for some of the Cl@Cd_iS_i nanoclusters and for Br@$Cd_{16}S_{16}$, which are too big to keep the guest atom at the center of their cavity. The charge of the trapped atom decreases as the size of the nanocluster increases. For these elements, the anionic structures are more stable than the neutral ones. In the case of Cl and Br, the stability increases as the size of the cluster increases.

The ab initio quantum dynamics simulations of these compounds reveal that the trapped atom moves around the center of the nanocluster as observed by the inspection of the values of R_{range}^{dyn} and R_{av}^{dyn} given in Table 3. We focus on Cl@$Cd_{12}S_{12}$ as a representative of the halogen-trapped endohedral compounds. It can be observed in Figure 4 that the total energy oscillates slightly around the average value during the whole simulation time, which is a fact that is very supportive of the thermal stability of the endohedral nanostructures. As seen earlier for the potassium, the Cl atom moves around the center of the cluster. Consequently, these compounds are predicted to be stable enough to survive long enough for their experimental detection.

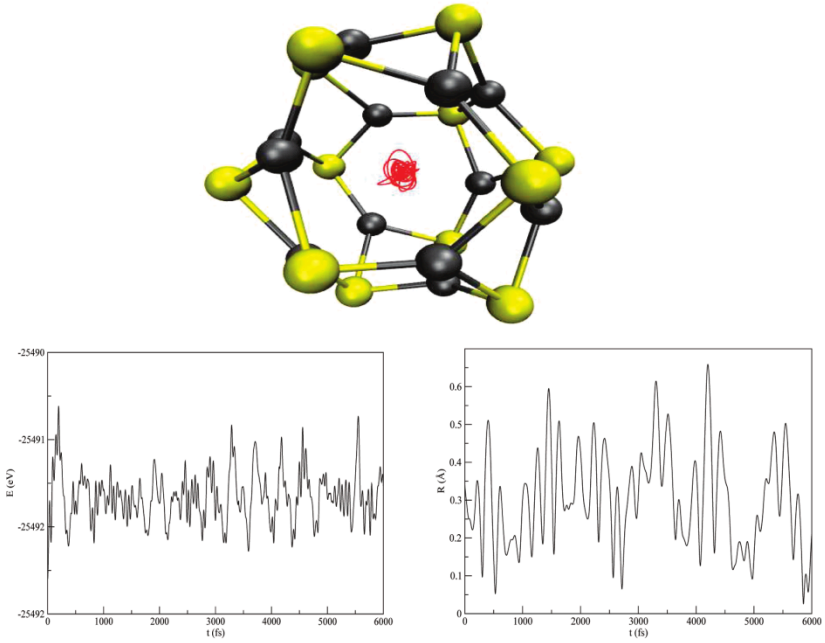

Figure 4. Dynamics simulation of Cl@$Cd_{12}S_{12}$. Top: Dynamical trajectories of the Cl atom inside the nanocluster. This plot was prepared as the K@$Cd_{12}S_{12}$ one. Below: The variation of the energy, in eV (left), and the variation of the distance, *R*, in Å (right), of the trapped K atom from the center of mass of the nanocluster as a function of time. S atoms are drawn in yellow, while Cd atoms are drawn in gray.

The calculated electron affinities of the halogen endohedral clusters are substantially larger than those of the corresponding guest atoms: EA(Cl) = 3.62 eV; EA(Br) = 3.36 eV. Hence, these endohedral nanoclusters may be seen as superhalogens (28) similarly to those of ZnS nanoclusters. It has been observed for electron affinities that EA (Cd_iS_i) < EA (X) < EA

($X@Cd_iS_i$) and for ionization energies that IE (K) ~ IE($K@Cd_iS_i$) < IE (Cd_iS_i). The isolated Cd*i*S*i* nanoclusters have a closed-shell electronic structure. When an alkali is trapped inside the cage, an electron is transferred to the lowest unoccupied molecular orbital (LUMO). This electron can more easily be removed than one from the highest occupied molecular orbital (HOMO) of the isolated cluster decreasing the ionization potential. Similarly, when a halogen atom is trapped, it takes an electron from the surface, and now the HOMO orbital is singly occupied therefore increasing the electron affinity with respect to the isolated cluster.

CONCLUSIONS

The geometrical structures and electronic and dynamic properties of the endohedral $(X@Cd_iS_i)^q$ i=9,12,15,16, q=0,± nanoclusters, with X standing either for the Na and K alkali elements or for the Cl and Br halogens, have been characterized by density functional theory and quantum molecular simulation calculations.

The stability of the resulting structures has been rationalized in terms of three parameters. The first is the appropriate matching between the size of the nanocluster, r_{cavity}, and the size of the trapped atom. The second is the shape of the nanocluster: the spherical nanoclusters are more prone to incarcerate atoms than the irregular ones. The third is the charge of the trapped atom: negatively charged guest atoms are the thermodynamically most stable ones. Because of the larger cavity size inside Cd_iS_i nanoclusters, in comparison to Zn_iS_i nanoclusters, Na is too small to lead to stable $X@Cd_iS_i$ compounds. This fact has been demonstrated by quantum dynamics calculations.

Encapsulation of halogen atoms results in endohedral nanoclusters with enhanced electron affinity relative to the guest halogen atom. These nanoclusters ought, therefore, to be considered as superhalogens in the same vein as the $X@Zn_iS_i$ and the $Al@Al_{12}$ nanoclusters, (29) where recent research has confirmed its predicted high electron affinity of EA = 3.20 eV as well as its ability to form salts with electropositive elements like potassium. (30) The Cl and Br endohedral nanoclusters studied in this work have electron affinities substantially larger than $Al@Al_{12}$, namely, EA > 4.5 eV. Hence, they are expected to have a stronger superhalogen character which makes them suitable to form ionic cluster-assembled materials. Furthermore, the electron affinities of the halogen endohedral nanoclusters and the ionization energies of the alkali endohedral nanoclusters of Cd_iS_i are rather similar. This is an interesting property since large IE/EA differences would yield substantial heat release during assembling that might destroy the assembled material as it is formed. Interestingly, $X@Zn_iS_i$ compounds were seen to have similar properties and recently were able to build stable cluster-assembled materials. (31)

Supporting Information

This material is available free of charge via the Internet at http://pubs.acs.org.

Corresponding Author

Elisa Jimenez-Izal - *Kimika Fakultatea, Euskal Herriko Unibertsitatea and Donostia International Physics Center (DIPC), P.K. 1072, 20018 Donostia, Euskadi Spain*; Email: elisa.jimenez@ehu.es

Authors

Jon M. Matxain - *Kimika Fakultatea, Euskal Herriko Unibertsitatea and Donostia International Physics Center (DIPC), P.K. 1072, 20018 Donostia, Euskadi Spain*

Mario Piris - *Kimika Fakultatea, Euskal Herriko Unibertsitatea and Donostia International Physics Center (DIPC), P.K. 1072, 20018 Donostia, Euskadi Spain*

Jesus M. Ugalde - *Kimika Fakultatea, Euskal Herriko Unibertsitatea and Donostia International Physics Center (DIPC), P.K. 1072, 20018 Donostia, Euskadi Spain*

Acknowledgment

This research was funded by Eusko Jaurlaritza (the Basque Government) SAIOTEK program. J.M.M. would like to thank the Spanish Ministry of Science and Innovation for funding through a “Ramon y Cajal” Fellowship. The SGI/IZO-SGIker UPV/EHU (supported by Fondo Social Europeo and MCyT) is gratefully acknowledged for generous allocation of computational resources.

References

(1) Sacher, E.; Meunier, M.; Luong, J. H. T.; Kabashin, A. V.;Sylvestre, J.-P.J. Am. Chem. Soc.2004,126, 7176.
(2) Heath, J. R.; O’Brien, S. C.; Zheng, Q.; Liu, Y.; Curl, R. F.; Kroto,H. W.; Tittel, F. K.; Smalley, R. E.J. Am. Chem. Soc.1985,107, 7779.
(3) Cioslowski, J.; Fleischmann, E.J. Chem. Phys.1991,94, 3730-3734.
(4) Nakane, T.Fullerene Sci. Technol.1997,5, 829–838.
(5) Dresselhaus, M. S.; Dresselhaus, G.; Eklund, P. C.Science ofFullerenes and Carbon Nanotubes; Academic Press: San Diego, CA, 1996.
(6) Forro, L.; Mihaly, L.Rep. Prog. Phys.2001,64, 649.
(7) Cardona, C. M.; Elliott, B.; Echegoyen, L.J. Am. Chem. Soc.2006,128, 6480.
(8) Wang, L. M.; Bulusu, S.; Zhai, H. J.; Zeng, X. C.; Wang, L. S.Angew. Chem., Int. Ed.2007,46, 2915.
(9) Cui, L.; Huang, X.; Wang, L.; Li, J.; Wang, L.Angew. Chem., Int.Ed.2007,46, 742.
(10) Matxain, J. M.; Piris, M.; Formoso, E.; Mercero, J. M.; Lopez, X.;Ugalde, J. M.ChemPhysChem2007,8, 2096.
(11) Scharfe, S.; Fa ¨ssler, T. F.; Stegmaier, S.; Hoffmann, S. D.; Ruhland,K.Chem.sEur. J.2008,14, 4479.
(12) Esenturk, E. N.; Fettinger, J.; Eichhorn, B. W.Chem. Commun.2005, 247.

(13) Esenturk, E. N.; Fettinger, J.; Eichhorn, B. W.J. Am. Chem. Soc.2006,128, 9178.
(14) Zhou, B.; Denning, M. S.; Kays, D. L.; Goicoechea, J. M.J. Am.Chem. Soc.2009,131, 2802.
(15) Wang, J.-Q.; Stegmaier, S.; Fa¨ssler, T. F.Angew. Chem., Int. Ed.2009,48, 1998–2002.
(16) Korber, N.Angew. Chem., Int. Ed.2009,48, 3216–3217.
(17) Hamad, S.; Catlow, C. R. A.; Spano, E.; Matxain, J. M.; Ugalde,J. M.J. Phys. Chem. B2005,109, 2703.
(18) Matxain, J. M.; Fowler, J. E.; Ugalde, J. M.Phys. ReV.A2000,61, 53201.
(19) Matxain, J. M.; Fowler, J. E.; Ugalde, J. M.Phys. ReV.A2000,62, 53201.
(20) Matxain, J. M.; Mercero, J. M.; Fowler, J. E.; Ugalde, J. M.Phys.ReV.A2001,64, 53201.
(21) Matxain, J. M.; Mercero, J. M.; Fowler, J. E.; Ugalde, J. M.J.Phys. Chem. A2003,107, 9981.
(22) Matxain, J. M.; Mercero, J. M.; Fowler, J. E.; Ugalde, J. M.J.Phys. Chem. A2004,108, 10502.
(23) Burnin, A.; Sanville, E.; BelBruno, J. J.J. Phys. Chem. A2005,109, 5026.
24) Sanville, E.; Burnin, A.; BelBruno, J. J.J. Phys. Chem. A2006,110, 2378.
(25) Kasuya, A.; et al.Nat. Mat.2004,3, 99.
(26) Liu, H.; Wang, S.; Zhou, G.; Wu, J.; Duan, W.J. Chem. Phys.2006,124, 174705.
(27) Matxain, J. M.; Formoso, E.; Mercero, J. M.; Piris, M.; Lopez, X.;Ugalde, J. M.Chem.sEur. J.2008,14, 8547.
(28) Matxain, J. M.; Eriksson, L. A.; Formoso, E.; Piris, M.; Ugalde,J. M.J. Phys. Chem. C2007,111, 3560.
(29) Fowler, J. E.; Ugalde, J. M.Phys. ReV.A1998,58, 383.
(30) Zheng, W. J.; Thomas, O. C.; Lippa, T. P.; Xua, S. J., Jr.; K., H. B.J. Chem. Phys.2006,124, 144304.
(31) Matxain, J. M.; Piris, M.; Lopez, X.; Ugalde, J. M.Chem.sEur. J.2009,15, 5138.
(32) Kasuya, A.; Noda1, Y.; Dmitruk, I.; Romanyuk, V.; Barnakov, Y.;Tohji, K.; Kumar, V.; Belosludov, R.; Kawazoe, Y.; Ohuchi, N.Eur. Phys.J. D2005,34, 39.
(33) Riehle, F. S.; Bienert, R.; Thomann, R.; Urban, G. A.; Kru¨ger, M.Nano Lett.2009,9, 514.
(34) Becke, A. D.Phys. ReV.A1988,38, 3098.
(35) Becke, A. D.J. Chem. Phys.1993,98, 5648–5652.
(36) Lee, C.; Yang, W.; Parr, R. G.Phys. ReV.B1988,37, 785.
(37) Kohn, W.; Sham, L. J.Phys. ReV.1965,140, A1133.
(38) Hohenberg, P.; Kohn, W.Phys. ReV.1964,136, B864.
(39) Stevens, W. J.; Krauss, M.; Basch, H.; Jasien, P. G.Can. J. Chem.1992,70, 612.
(40) Soler, J. M.; Artacho, E.; Gale, J. D.; Garcia, A.; Junquera, J.;Ordejon, P.; Sanchez-Portal, D.J. Phys.: Condens. Matter2002,14, 2745.
(41) Perdew, J.; Burke, K.; Ernzerhof, M.Phys. ReV. Lett.1996,77,3865.
(42) Zhang, Y.; Yang, W.Phys. ReV. Lett.1998,80, 890.
(43) Hammer, B.; Hansen, L. B.; Norskov, J. K.Phys. ReV.B1999,59,7413.
(44) Troullier, N.; Martins, J. L.Phys. ReV.B1991,43, 1993.
(45) Kleinman, L.; Bylander, D. M.Phys. ReV. Lett.1982,48, 1425.